Dendrite-like Self-assembly of Magnetite Nanoparticles on Porous Silicon**

Sivakumar Balakrishnan, Yurii K. Gun'ko,* Tatiana S. Perova, Robert A. Moore, Munuswamy Venkatesan, Alexios P. Douvalis and Paul Brouke.

[*] S. Balakrishnan, Dr. Y. K. Gun'ko

School of Chemistry, Trinity College Dublin, Dublin 2 (Ireland)

Fax: (+353)1-6712826

E-mail: igounko@tcd.ie

Dr. T. S. Perova, Dr. R. A. Moore

Department of Electronic & Electrical Engineering, University of Dublin, Trinity College, Dublin 2 (Ireland)

Dr. M. Venkatesan

School of Physics, Trinity College, University of Dublin, Dublin 2 (Ireland)

Dr. A. P. Douvalis

Department of Materials Science and Engineering, University of Ioannina, P.O. Box 1186, 45110, Ioannina (Greece)

Dr. P. Brouke

Swinburne University of Technology, PO Box 218, Hawthorn, Victoria 3122 (Australia)

Hierarchical assembly of nanoparticles is very important for the development of bottom–up approaches in technology. The self-organisation of nanoparticles has been studied extensively and the preparation of novel nanostructured material is an emerging topic in the field of advanced materials.[1] The self-assembly of nanoparticulate materials strongly depends on inter-particle interactions, particle size distribution [2] and particle shape.[3] The process of assembly of nanoparticles can result in different patterns such as rings, rods or needles. [4] The different shapes and morphologies of the particle assemblies depend on the dipole-dipole and other interactions between individual particles and also on the interfacial processes involving the substrate and the nanoparticles. It has been reported that by varying the conditions for nanocrystal deposition on substrates, a variety of organised structures can be prepared.[3] There are several reports on fractal structures formed by metal particles including one on forming fractal silver nanocrystallites by using γ-radiation in the presence of solvents.[5] It has been proven theoretically that the formation of fractal structures on solid substrates does have some dependence on the roughness of the substrate.[6] The theoretical and mathematical basis for the formation of fractal structures has been well developed.[7] Recently magnetic Fe_3O_4 fractal nanocrystals have been synthesised by a solvothermal process.[8] Cao *et al* have also reported the preparation of single- crystal fractals of magnetic α-Fe_2O_3 using hydrothermal reactions.[9] Magnetic nanoparticles are widely studied for their application in various fields such as information storage,[10] colour imaging,[11] bioprocessing [12] and in controlled drug delivery.[13] Therefore, self-organisation of magnetic nanostructured materials into fractal structures is a very important aspect of nanotechnology and modern materials science.

In this communication, we report for the first time the self-organisation of magnetic Fe_3O_4 nanoparticles into fractal dendrite-like structures using porous silicon (PSi) as a substrate. In contrast to the recently reported [8] surfactant assisted solvothermal preparation of magnetite fractal nanocrystals, our approach is relatively simple and does not require the use of high temperature and pressure or any

surfactants. Also, all reagents, materials and equipment used in our preparation are readily accessible. The magnetite nanoparticles arranged on porous silicon templates were characterised by micro-Raman spectroscopy, scanning electron microscopy (SEM), transmission electron microscopy (TEM), X-ray diffractometry (XRD), Mossbauer spectroscopy and magnetic measurements (SQUID).

Porous silicon has been a subject of numerous and detailed studies as a very promising host material for the development of new composites. [14] The uses of porous silicon arise mainly from utilising its optical and surface properties. Porous silicon has found applications in sensors, reflectors, silicon lithography, electronic and micro-mechanical devices and in biomedicine.[15] The objective of our work was to investigate porous silicon as a potential substrate for the preparation of magnetic nanoparticle assemblies.

In this work, a porous silicon sample was prepared by electrochemical etching of a (100) p- silicon wafer with resistivity, ρ = 10 ohm cm, in 4% HF in DMF electrolyte solution at a current density, J = 7.7 mA/cm^2, for 6 hours. Pore depth was found to be 10 microns. SEM images of the PS sample are presented in Figure 1 below (see also Supporting Information). From the SEM images it is quite clear that the macroporous silicon surface has fractal-like morphology. There have been several reports describing the formation of porous silicon nanostructures using fractal models.[15] According to these models the porous Si surfaces can be considered as self-affine fractal structures. For example porous silicon can be presented as a set of clusters of silicon atoms surrounded by silicon oxides, whereas the single crystalline silicon substrate can be considered as an infinite cluster. [16] The formulae for the estimation of variable porosity of silicon and the forbidden bandgap value of clusters have been suggested as functions of sizes of nanocrystallites. Thus the fractal-like morphology of our porous silicon sample can be explained using these models. The mechanism of silicon electroetching is still not fully understood and different theoretical models for etching such as the Current Burst Model (CBM) and the Space Charge Region (SCR) models have been proposed. [17, 18] The CBM postulates that current flow across the solid silicon/HF-containing electrolyte interface is spatially and temporally

inhomogeneous. Local current (called the current burst) starts to flow whenever the local field strength is high enough. This current generates some oxide growth and it stops the flow at certain thickness of the oxide. Then, the oxide is dissolved (via chemical process) and whenever the oxide layer is thin enough, the cycle starts again. [17] In the SCR model the pore formation involves the formation of hydrogen terminated space charge region, which acts as a passivating layer. [18]

The fractal-patterned porous silicon sample (Figure 1) with the hydroxyl-terminated surface was then used as a substrate for deposition of magnetic Fe_3O_4 nanoparticles. The process was performed by well-documented co-precipitation of magnetite particles from a solution of iron (Fe^{3+}/Fe^{2+}) salts in the stoichiometric ratio ($Fe^{3+}/Fe^{2+} = 2$) using aqueous ammonia in the presence of the porous silicon substrate.[19] The black precipitate formed together with porous silicon samples was washed off several times with water and organic solvents and dried in vacuum. A schematic representation of the process is given in Scheme 1 below.
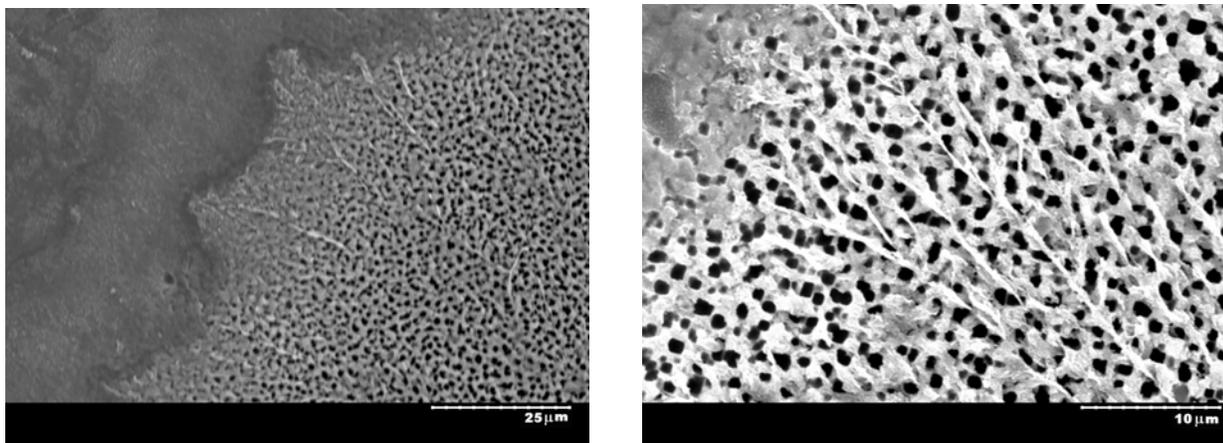
Figure 1. SEM images of porous silicon sample used in present studies.
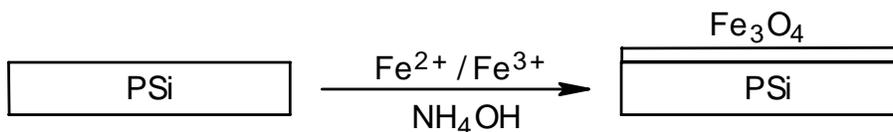
Scheme 1. Schematic representation of the preparation of porous silicon–magnetite composite.

Both the loose dried black powder and porous silicon composite were characterised using XRD (Figure 2). Reflections of both the XRD patterns showed *d* spacing values and relative peak intensities that coincide exactly with JCPDS data of magnetite (Fe_3O_4). The XRD patterns of porous silicon composites also contained strong reflections corresponding to the Si (100) substrate (2θ at 69.6°). Some of the reflections for magnetite overlap with those of porous silicon (the 2θ peak of magnetite at 71.3° is overlapped by the broad peak from porous silicon represented by an asterisk). The particle sizes for both loose magnetite powder and magnetite-porous silicon composites were calculated using the Debye-Scherrer formula [20] giving a particle diameter of 7 ± 2 nm in both cases. The porous silicon-magnetite composite was also characterised by micro-Raman spectroscopy (see Supporting Information). The Raman spectrum of the PS–magnetite sample shows peak positions at 520 cm^{-1} and 668 cm^{-1}. The peak position at 520 cm^{-1} corresponds to the silicon [21] and the peak at 668 cm^{-1} corresponds to the magnetite. [22]
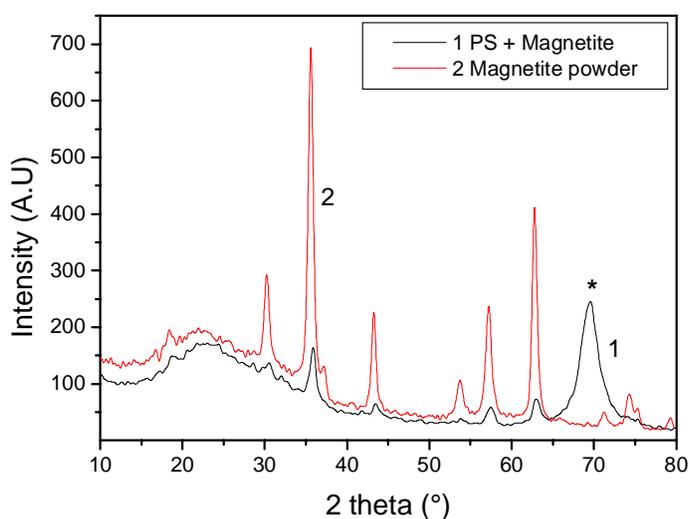
Figure 2. XRD patterns of PSi-magnetite composite (1) and loose magnetite particles (2).

The room temperature magnetisation curve for porous silicon–magnetite composite material is presented in Figure 3. The room-temperature magnetisation (σ) of 43 Am^2Kg^{-1} in a field of 1 T is considerably lower than the room temperature saturation magnetisation (*ca*. 90 Am^2Kg^{-1}) of bulk Fe_3O_4.[23] The reduction and lack of saturation could be attributed to the particle size effect. If a specimen consists of small particles, its total magnetization decreases with decreasing particle size due to the increased dispersion in the exchange integral [24] and ultimately reaches the superparamagnetic state, when each particle acts as a big 'spin' with suppressed exchange interaction between particles. Thus, the magnetisation results revealed that the magnetite particles demonstrate superparamagnetic behaviour.
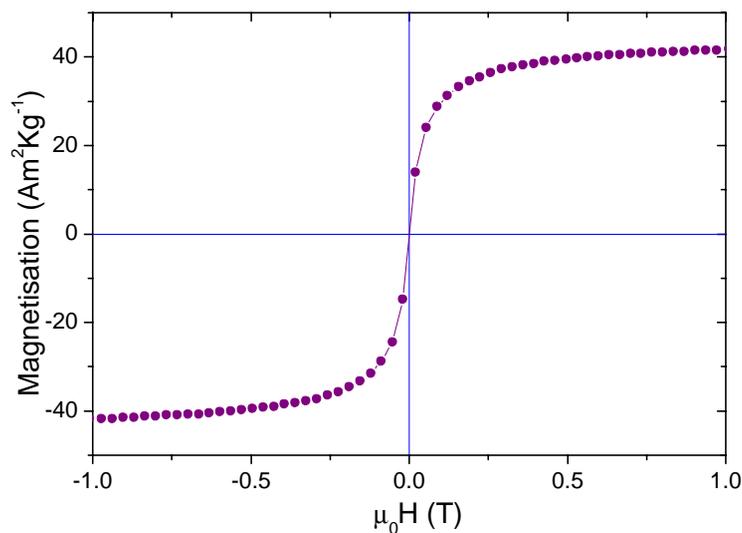
Figure 3. Magnetization curve of magnetite–porous silicon composite measured at RT.

Mössbauer spectra (MS) recorded at 300 K, 150 K, and 77 K for both the PS-magnetite and the unsupported magnetite nanoparticles samples are compared in Figure 4. On initial inspection, the spectral shape of the two samples at the same temperature looks very similar. At all temperatures, in particular at 300 K, the spectral lines for both samples are quite broad and asymmetric. Consequently,

four sextets are required to describe the magnetite hyperfine structure for both samples. At 300 K and 150 K, the IS values for all components are quite close to each other. They lie in the range 0.35 mms^{-1} – 0.43 mms^{-1} at 300 K, and 0.39 mms^{-1} – 0.46 mms^{-1} at 150 K. The corresponding hyperfine magnetic field (B_{hf}) values range between 27.0 T and 47.1 T at 300 K, and between 44.5 T and 52.0 T at 150 K for both samples. The difference in the B_{hf} values between the four components reflects the distribution of particle sizes. The reduction of the B_{hf} values compared with the corresponding values of bulk magnetite is attributed to particle size effects. Thermal fluctuation influences the shape of Mössbauer spectrum more profoundly for smaller particles as their B_{hf} values reduce significantly.[24-28] At 77 K three out of the four components have very similar IS values with a weighted average of around 0.45 mms^{-1} and both samples have increased B_{hf} values between 49.0 T and 53.2 T. The fourth component in each spectrum, which has a lower absorption area (6 – 8%), possesses a higher IS value around 0.63 mms^{-1}, while its B_{hf} value remains at 45.0 T for both samples. The more divalent character for this fourth component reflects the onset of some charge ordering in the magnetite particles below the Verwey transition.[26] For both samples all quadrupole shift (2ε) values are close to zero for all components at all temperatures studied.

The line broadening and asymmetry is a striking feature of the MS of magnetite particles with distributions of particle size in the range of a few tenths of nanometers.[24-28] However the lack of a contribution from a temperature independent paramagnetic component in the MS of Figure 5 indicates that the particle sizes exceed the limit to produce super-paramagnetic behaviour. The upper size limit of magnetite nanoparticles for the appearance of super-paramagnetism, monitored as a contribution from a paramagnetic component to the MS at RT, is about 6 to 10 nm.[24-28] Thus, the major contribution to the MS arises from particles with sizes of a few tenths of nanometers. On the other hand, the observed line broadening also indicates very small contributions from micron-sized particles. This is confirmed by the absence of narrow and symmetric lines, resembling the spectrum of bulk magnetite in the MS at RT.
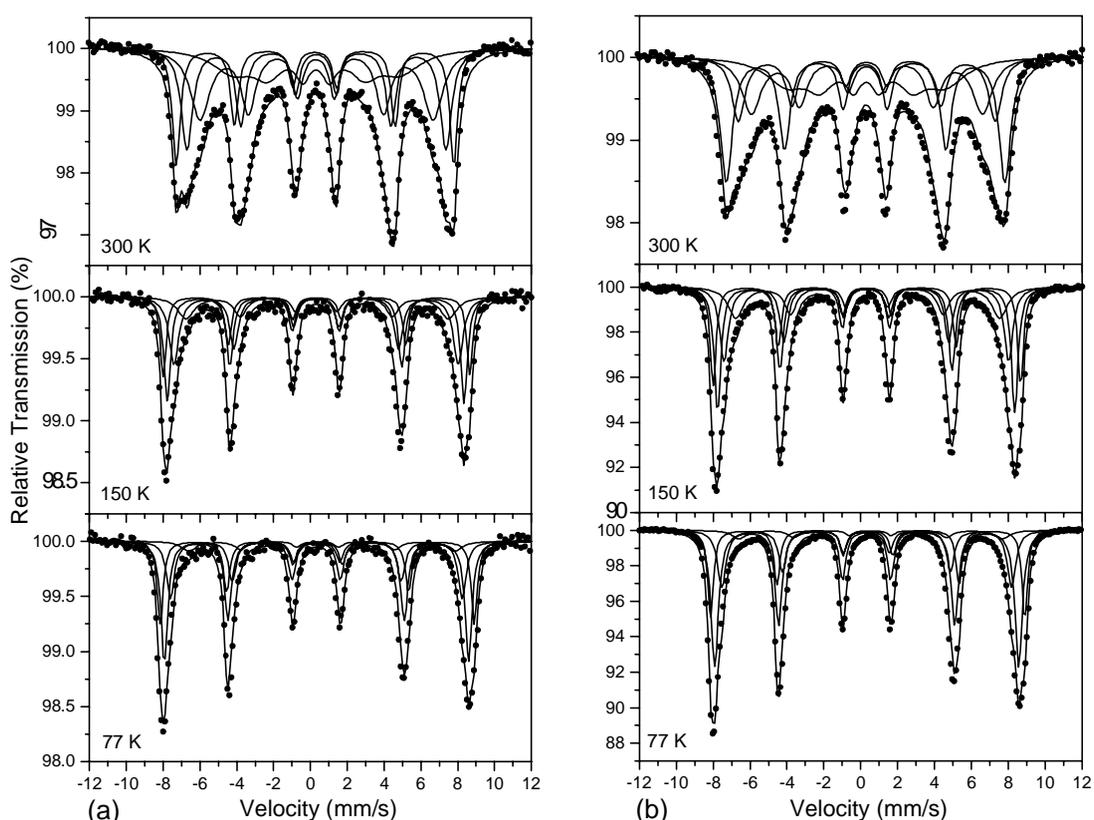
Figure 4. Mössbauer spectra of magnetite particles (a) on porous Si, and (b) loose particles, recorded at different temperatures.

From analysis of the Mössbauer data, it is evident that both the porous silicon-magnetite composite and magnetite nanoparticles show no major differences in their particle size distribution. This is confirmed further by other characterisation techniques *viz*., electron microscopy and x-ray diffraction.

The morphology of the porous silicon-magnetite composite material was studied using SEM (Figure 5). The SEM images showed fractal-like or dendrite-like morphology of magnetite nanoparticles deposited on the porous silicon top surface. Magnified SEM images have clearly shown that each branch of the fractal consists of micron-sized particles assembled in strings. The presence of iron in the magnetite fractal structure was confirmed by energy dispersive X-ray spectroscopy (see supporting information).
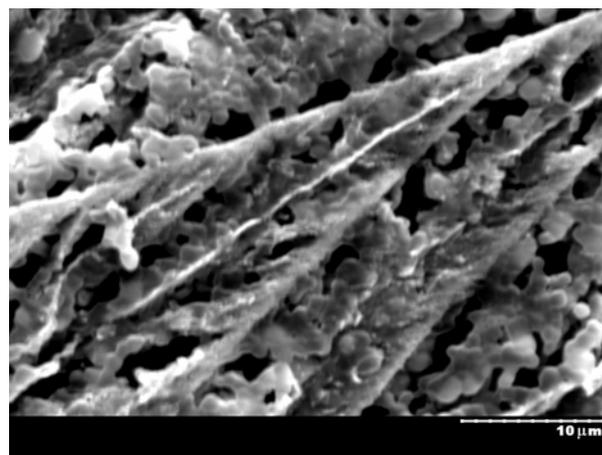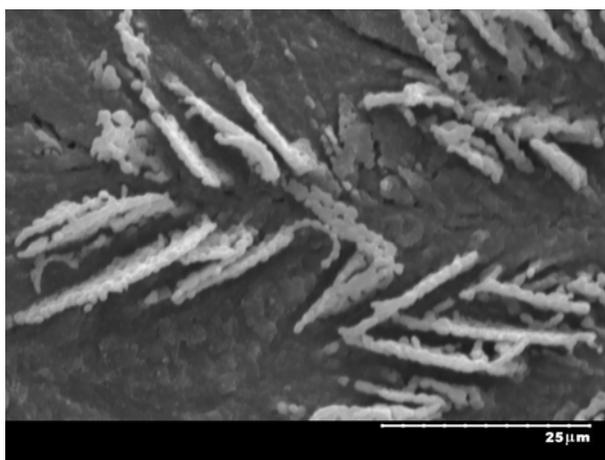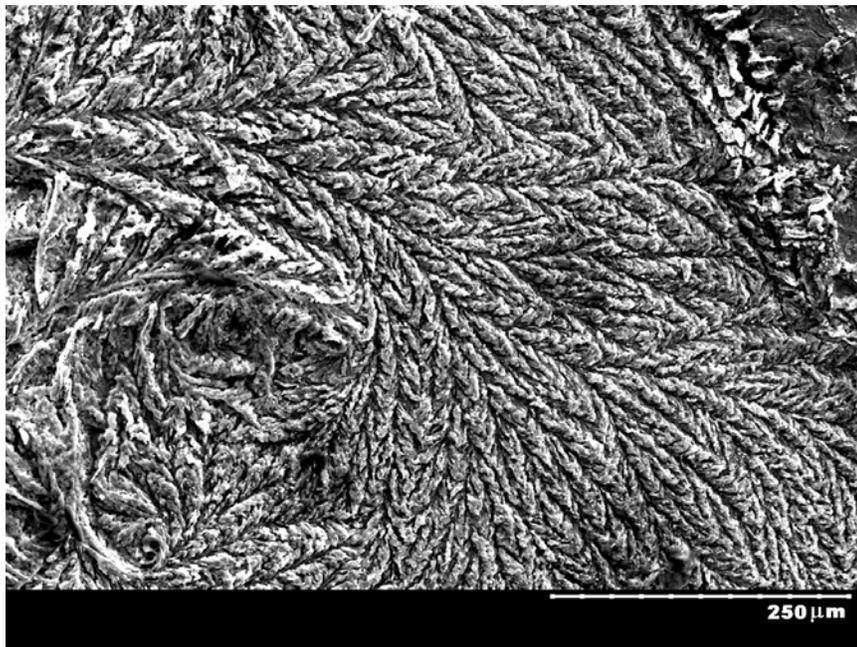
Figure 5. SEM images of PSi–magnetite sample at different magnifications.

The optical images and the cross-sectional SEM images of porous silicon-magnetite composite also showed the fractal morphology and the depth to which the magnetite particles partially penetrated into the pores of silicon (see Supporting Information). TEM imaging of the magnetite powder scratched off from the porous silicon surface clearly shows nanoparticles in the 6- 12 nm range (Figure 6). These results agree quite well with the results calculated using the Debye-Scherrer formula and the

Mössbauer spectroscopy results above. The TEM images of loose magnetite powder have shown very similar particle size and distribution. In overall all characteristics (XRD, TEM images, Raman and Mössbauer spectra), of unsupported magnetite particles were identical to those of magnetite on the porous silicon surface.
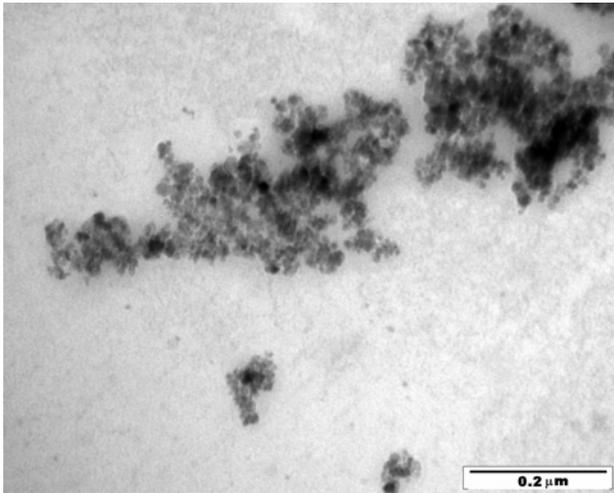
Figure 6. TEM image of the magnetite nanoparticles scratched off the PSi surface.

The fractal formation and side branching depends on the nanocrystal anisotropy and the growth mechanism. In our samples the magnetite branches are long and narrow, which is characteristic of limited edge diffusion. Thus, growth of magnetite dendrites is within the framework of a Diffusion Limited Aggregation (DLA) model with a fixed fractal dimension. [29] DLA model involves cluster formation by the adhesion of a particle with a random path on contact with a selected seed, thus allowing the particle to diffuse and stick to the growing structure. The growth of a DLA cluster is determined by the set of growth probabilities {P_i} (P_i is the next unit to be added to the cluster). [30] In our case the fractal-like pre-patterned porous silicon surface serves as a template which controls the morphology and dimensions of dendritic structures at the solid-liquid interface. We have implemented the Variogram method [31] of fractal dimension estimation for both original porous silicon substrate and magnetite fractals. Calculations for original porous silicon substrate gave the slope of 1.605 and

the fractal dimension of 2.2, and estimations for magnetite fractal on porous silicon resulted in the slope of 1.625 and the fractal dimension of 2.19. According to these data the magnetite fractal dimension is the same as one for the original porous silicon substrate. This shows a clear correlation between the dimension and morphology of the fractal pattern on original porous silicon substrate and the magnetite fractal. Obviously, the presence of self-organised pores on the substrate restricts the diffusion of the particles (DLA regime) on the porous silicon surface providing a certain pattern for morphology and dimensions of the magnetite fractal.

In conclusion, we have found that co-precipitation of magnetite nanoparticles in the presence of hydroxyl functionalised porous silicon samples resulted in the self-organisation of magnetite nanoparticles into dendrite- or fractal-like structures, yielding new magnetic composites. This magnetic fractal preparation technique is relatively simple and not technically demanding. The magnetic nanoparticles that formed the fractals have clearly demonstrated superparamagnetic behaviour. The mechanism of the fractal formation involves a DLA growth model influenced by the porous substrate effect. These factors also control the dimension and morphology of the magnetite fractal. Magnetic fractals add an additional new dimension to nanoscale spin electronics as each small portion of the fractal can be viewed as a reduced-scale replica of the whole. These fractals are considered to exist in partial or fractional dimension and produce a magnetic field that exhibits fractal behaviour. Magnetite is an excellent magnetic material with a high Curie temperature and stable room temperature magnetoresistance, therefore magnetite fractals, which demonstrate self similarity and order across scales can provide new paths to low-cost high density storage media. They are potentially useful in future technological applications such as data storage and information analysis. In addition both porous silicon and magnetite are biocompatible materials. These new magnetite-porous silicon composites might find potential applications in biotechnology as biomagnetic implants in medicine and substrates in cell biology. We also believe that porous silicon and potentially other similar porous materials can

be used as substrates for controlled growth of fractal structures for various (not only magnetic iron oxide) nanomaterials. This may open up new approaches in the preparation and self-organisation of nanoparticles and result in novel nano- and micro- structured composite materials with interesting properties and broad range of applications.

Experimental section

The p-type silicon samples used for the present investigation were prepared by electrochemical etching of silicon {CZ, (100), ρ = 10 ohm cm, Current density, J = 7.7 mA/cm^2, time = 6 hours} in 4% HF in DMF electrolyte solution.

The as-fabricated porous silicon samples were first etched with HF (2 wt%) and then functionalised with hydroxyl groups, as reported. [32] The magnetite nanoparticles were prepared according to published procedures [19] with slight modifications. In brief, $FeCl_2$ and $FeCl_3$ were weighted by maintaining the stoichiometry of Fe^{3+}/Fe^{2+} equal to 2. Both were dissolved in 100 ml of 1.0 M sodium chloride aqueous solution (deoxygenated water) under argon. Sodium chloride was used to adjust the ionic strength of the iron solution. The above solution was placed in a water-bath preheated to 25°C with sonicating. The hydroxyl functionalised porous silicon samples were introduced to this magnetite solution prior to precipitation. Concentrated ammonia solution was added in drops until the pH reached 9. The dark precipitate together with the silicon samples were washed with double distilled deoxygenated water three times followed by diethyl ether and ethanol. The sample was then dried under vacuum for 9-10 hours.

Room temperature micro-Raman spectra were measured with a Renishaw 1000 micro-Raman system. The excitation wavelength was 514.5 nm from an Ar+ ion laser (Laser Physics Reliant 150 Select Multi-Line) with a typical laser power of ~ 10 mW in order to avoid excessive heating. The 50x-magnifying objective of the Leica microscope focused the beam into a spot of about 1 µm in diameter. SEM equipment used was an S-3500N variable pressure scanning electron microscope (Hitachi, Japan),

which was operated at 20.0 kV. The transmission electron microscopy (TEM) images were taken on a Hitachi H-7000 microscope. The TEM was operated at a beam voltage of 100 kV. Samples for TEM were prepared by the deposition and drying of a drop of the powder dispersed in ethanol onto a formvar coated 400 mesh copper grid. Magnetic measurements were carried out both at room temperature using a MPMS superconducting quantum interference device (SQUID) magnetometer. The XRD in this work was carried out using a Siemens D-500 X-ray diffractometer. X-ray patterns from powder samples were taken in reflection mode. Mössbauer spectra were collected at sample temperatures of 300 K, 150 K and 77 K, in transmission geometry using a constant acceleration spectrometer equipped with a ^{57}Co(Rh) source kept at RT. The velocity calibration was done using α-Fe and all isomer shift (IS) values are given relative to α-Fe at RT.

_____

 [1] L.-Q. Wang, G. J. Exarhos, J. Liu, *Adv. Mater*. **1999**, 11, 1331-1341.

[2] a) C. P. Collier, T. Vossmeyer, J. R. Heath, *Annu. Rev. Phys. Chem.* **1998**, 49, 371-404; b) M. P. Pileni, *J. Phys. Chem. B*. **2001**, 105, 3358-3371.

[3] N. R. Jana, *Angew. Chem. Int. Ed*. **2004**, 43, 1536-1540.

[4] a) B. Nikoobakht, Z. L. Wang, M. A. El-Sayed, *J. Phys. Chem. B* **2000**, 104, 8635-8640; b) F. Kim, S. Kwan, J. Akana, P. Yang, *J. Am. Chem. Soc*. **2001**, 123, 4360-4361; c) J. Fang, A. Kumbhar, W. L. Zhou, K. L. Stokes, *Mater. Res. Bull*. **2003**, 38, 461-467.

[5] Q. Yang, F. Wang, K.Tang, C. Wang, Z. Chen, Y. Qian, *Mater. Chem. Phys*. **2002**, 78, 495-500.

[6] E. Rabani, D. R. Reichman, P. L. Geissler, L. E. Brus, *Nature* **2003**, 426, 271-274.

[7] B. B. Mandelbrot, *Fractals and Chaos*, Springer, New York, **2004**.

[8] G. Zou, K. Xiong, C. Jiang, H. Li, T. Li, J. Du, Y. Qian, *J. Phys. Chem. B*. **2005**, 109, 18356-18360.

[9] M. Cao, T. Liu, S. Gao, G. Sun, X. Wu, C. Hu, Z.L. Wang, *Angew. Chem. Int. Ed*. **2005**, 44, 4197-

4201.

[10] A. G. Audram, A. P. Huguenard, *U. S. Patent*, **1981**, 4,302,523.

[11] R. F. Ziolo, *U. S. Patent*, **1984**, 4,474,866.

[12] N. M. Pope, R. C. Alsop, Y. –A. Chang, A. K. Sonith, *J. Biomed. Mater. Res*. **1994**, 28, 449-457.

[13] S. P. Bhatnagar, R. E. Rosenweig, *J. Magn. Magn. Mater*. **1995**, 149, 198-198.

[14] A. Moadhen, H. Elhouichet, M. Oueslati, M. Ferid, *J. Lumin*. **2002**, 99, 13.

[15] V. Lehmann, The Electrochemistry of Silicon, Wiley-VCH, Weinheim, Germany, **2002**.

[16] a) Y. Park, *Fractals-Complex Geometry Patterns and Scaling in Nature and Society*. **2000**, 8, 301-306; b) O. B. Isayeva, M. V. Eliseev, A. G. Rozhnev, N. M. Ryskin, *Solid-State Electron*. **2001**, 45, 871-877; c) T. Nychyporuk, V. Lysenko, D. Barbier, *Phys. Rev. B*. **2005**, 71, 115402-115405; d) V. M. Aroutiounian, M. Zh. Ghoolinian, H. Tributsch, *Appl. Surf. Sci*. **2000**, 162-163, 122-132.

[17] H. Föll, M. Christophersen, J. Carstensen and G. Haase, *Mater. Sci. Eng*. **2002**, R39, 93.

[18] V. Lehmann and H. Föll, *J. Electrochem. Soc*. **1990**, 137, 653.

[19] X. –P. Qiu, *Chin. Journ. Chem*. **2000**, 18, 834-837.

[20] A.R. West, *Solid State Chemistry and its Applications*, John Wiley & Sons, London, **1984**, 174.

[21] V. Craciun, C. B. -Leborgne, E. J. Nicholls, I. W. Boyd, *Appl. Phys. Lett*. **1996**, 69, 1506-1508.

[22] A. Wang, L. A. Haskin, B. L. Jollif, *Lunar Planet Sci*. **1998**, 29, 1819-1820.

[23] J. M. D. Coey, A. H. Morrish, G. A. Sawatzky, *J. de Physique*. **1971**, 32, C1.

[24] S. H. Gee, Y. K. Hong, D. W. Erickson, M. H. Park, *J. Appl. Phys*. **2003**, 93, 7560-7562.

[25] a) S. Mørup, H. Topsøe and J. Lipka, *J. de Physique*. **1976**, 37, C6-287; b) S. Mørup, H. Topsøe, *Appl. Phys*. **1976**, 11, 63-66.

[26] G. F. Goya, T. S. Berquo, F. C. Fontera, *J. Appl. Phys*., **2003**, 94, 3520-3528.

[27] S. A. Corr, Y. K. Gun'ko, A. P. Douvalis, M. Venkatesan, R. D. Gunning, *J. Mater. Chem*. **2004**, 14, 944-946.

[28] P. Roggwiller, W. Kunding, *Sol. State Comm.* **1973**, 12, 901-903.

[29] T.A. Witten, L.M. Sander, *Phys. Rev. Lett.* **1981**, 47, 1400.

[30] T. C. Halsey, *Phys. Rev. Lett.* **1997**, 78, 9, 1719-1722.

[31] J. Kolibal, J. Monde, *Computers & Geosci.* **1998**, 24, 785-795.

[32] R. Cohen, N. Zenou, D. Cahen, S. Yitzchaik, *Chem. Phys. Lett.* **1997**, 279, 270-274.